Crystal Structure of Sulerythrin, a Rubrerythrin-Like Protein from a Strictly Aerobic Archaeon, *Sulfolobus tokodaii* Strain 7, Shows Unexpected Domain Swapping[†,‡]

Shinya Fushinobu,* Hirofumi Shoun, and Takayoshi Wakagi

Department of Biotechnology, The University of Tokyo, 1-1-1 Yayoi, Bunkyo-ku, Tokyo 113-8657, Japan

Received February 7, 2003; Revised Manuscript Received August 7, 2003

ABSTRACT: Sulerythrin is the first rubrerythrin-like protein to be isolated from an aerobic organism, *Sulfolobus tokodaii* strain 7, and it lacks a C-terminal rubredoxin-like FeS_4 domain. The protein purified from *Sulfolobus* cells was crystallized, and the crystal structure was determined at 1.7 Å resolution. The dimer of sulerythrin exhibited "domain-swapping" at the loop connecting αB and αC, hybrid four-helix bundles consisting of αA/B and αC/D being formed. The structure and atomic identity of the binuclear metal center were determined by means of anomalous scattering analysis. The site contained 1.0 mol of hexacoordinate Fe, 0.80−0.87 mol of tetracoordinate Zn, and 0.73−0.88 mol of putative O_2 per monomer. The metal ions were found at exchanged positions compared to those in the Fe/Zn-containing rubrerythrin from *Desulfovibrio vulgaris*. The results demonstrate that the binuclear metal center of rubrerythrin-like proteins is plastic in its ability to bind metal ions.

Rubrerythrin is a non-heme iron homodimeric protein containing both a hemerythrin-like binuclear iron cluster and a rubredoxin-like FeS_4 center in each subunit (*1*, *2*). It was first found in *Desulfovibrio vulgaris*, and subsequently found in other obligatory anaerobes, such as *Clostridium* and *Porphyromonas* species (*3*−*5*). *D. vulgaris* contains a second rubrerythrin-like protein, called nigerythrin (*6*, *7*). Recent genome analysis of other organisms revealed that rubrerythrin-like proteins are present in both archaea and bacteria (Figure 1). However, all the sources are anaerobes except for the *Sulfolobus* species and *Cyanophora*. Among the rubrerythrin-like proteins, rubrerythrin from the periplasmic cellular fraction of *D. vulgaris* (Rbr)[1] (*8*) has been extensively studied. A number of enzymatic activities of rubrerythrin, such as inorganic pyrophosphatase (*9*), ferroxidase (*10*), superoxide dismutase (*3*), and oxygen reductase (*11*) activities, have been reported. Within the past few years, reduced (all-ferrous) Rbr ($2Fe-Rbr_{red}$) has been implicated as hydrogen peroxide reductase (peroxidase) in a novel oxidative stress protection system (*12*−*14*). However, the reproducibility and physiological relevance of some of these activities remain to be considered (*7*, *15*−*17*).

Several early studies indicated that the binuclear metal center of both Rbr and nigerythrin, as isolated from *D. vulgaris*, is an oxo-bridged di-iron site (*1*, *7*, *18*). Many subsequent biochemical and crystallographic studies on Rbr have been conducted on a recombinant protein reconstituted with exogenous iron (*19*−*22*). In the crystal structure of oxidized (all-ferric) Rbr ($2Fe-Rbr_{ox}$; entry 1LKM in the Protein Data Bank), the binuclear metal center is a μ-oxo bridged di-iron site (*21*, *22*). In the $2Fe-Rbr_{red}$ structure (1LKO, reduced all-ferrous form), one of the Fe atom has moved 1.8 Å, and two waters are bound. Moreover, the structure of the azide adduct of $2Fe-Rbr_{red}$ has been determined. On the basis of these 2Fe−Rbr structures, a mechanism for hydrogen peroxide activity has been proposed (*22*). However, the metal content of the binuclear metal center of Rbr is controversial. Sieker et al. claimed that the native Rbr, as isolated from *D. vulgaris* under aerobic conditions, contains Fe and Zn atoms in its binuclear metal center, and presented the crystal structure of the Fe/Zn form of Rbr ($Fe/Zn-Rbr_{aero}$; 1DVB) (*23*, *24*). In a recent study, the native Rbr structure, which was obtained under anaerobic conditions ($Fe/Zn-Rbr_{anaero}$; 1JYB), was found to have an Fe/Zn center with a zinc position differing from that of $Fe/Zn-Rbr_{aero}$ (*25*). When the crystal was exposed to air, the zinc atom moved, and the pyrophosphatase activity increased gradually. Therefore, the binuclear metal center of Rbr was shown to be plastic in its ability to bind metals in at least four different states without a large structural change.

Recently, we isolated a rubrerythrin-like protein from a strictly aerobic and thermoacidophilic archaeon, *Sulfolobus tokodaii* strain 7, and biochemically characterized it and named it sulerythrin (*26*). It was the first rubrerythrin-like protein isolated from an aerobic organism. Sulerythrin is a homodimer of 16 278 Da, which consists of the gene product of the ORF, st2370 (144 aa), recently found on genome analysis of the organism (*27*). The protein lacks a C-terminal rubredoxin-like FeS_4 domain, and shows similar spectroscopic characteristics to "chopped" rubrerythrin (18 349 Da) (*26*), which was artificially designed to delete the C-terminal domain (residues 151−220) of Rbr (24 387 Da/220 residues) (*19*). The metal content was determined to be 0.76 mol of

[†] This work was supported by the National Project on Protein Structural and Functional Analysis, and the TARA (Tsukuba Advanced Research Alliance) Sakabe Project.

[‡] The Brookhaven Protein Data Bank code is 1J30.

* To whom correspondence should be addressed. Phone: +81 3 5841 5151. Fax: +81 3 5841 5337. E-mail: asfushi@mail.ecc.u-tokyo.ac.jp.

[1] Abbreviations: Rbr, *Desulfovibrio vulgaris* rubrerythrin; $2Fe-Rbr_{ox}$, all-ferric Rbr; $2Fe-Rbr_{red}$, all-ferrous Rbr; $Fe/Zn-Rbr_{aero}$, aerobically prepared Rbr containing Fe/Zn; $Fe/Zn-Rbr_{anaero}$, anaerobically prepared Rbr containing Fe/Zn.

10.1021/bi034220b CCC: $25.00
Published on Web 09/17/2003

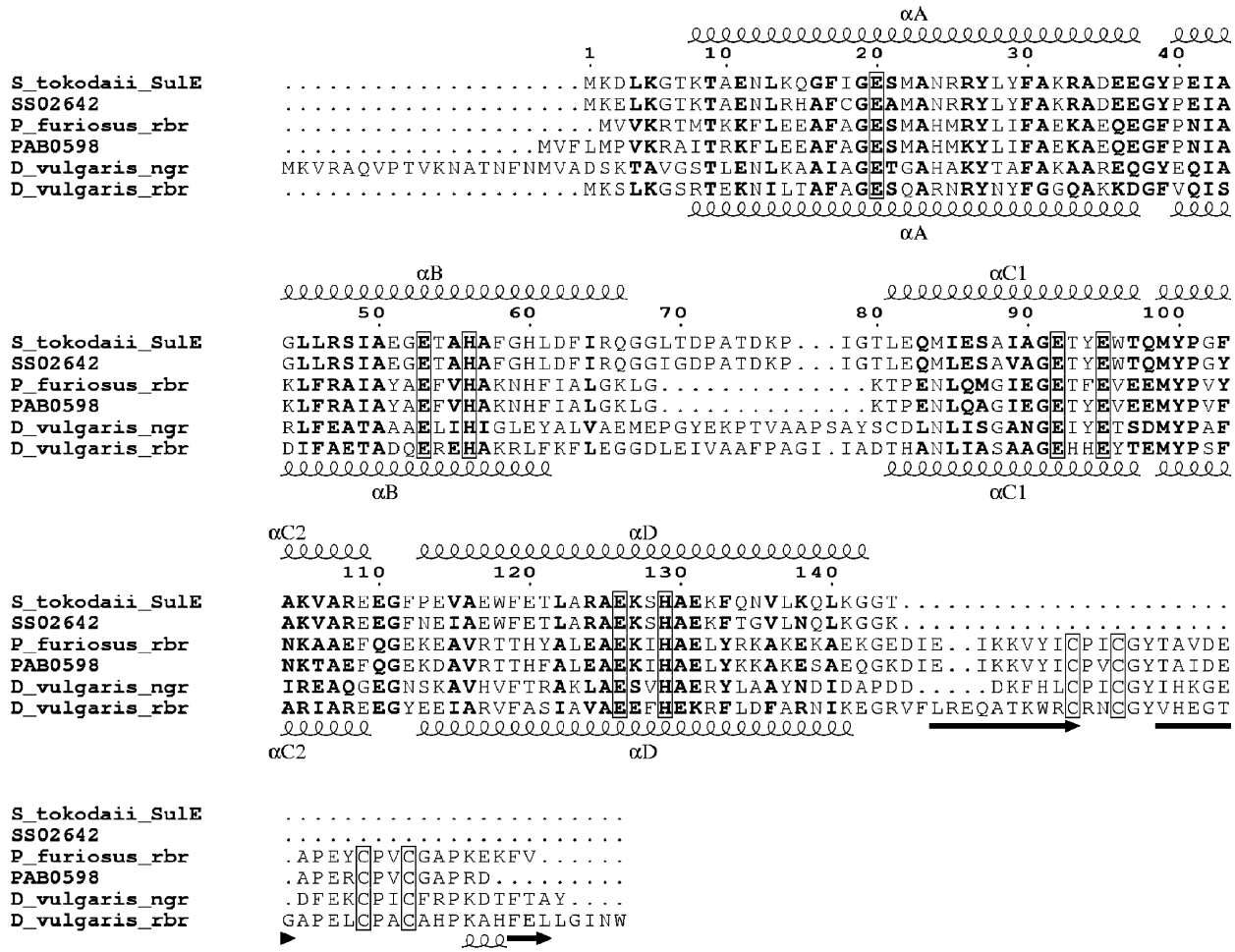

FIGURE 1: Amino acid sequence alignment of sulerythrin and rubrerythrin-like proteins. Residues liganded to metal centers and other highly conserved residues are boxed and shown in bold, respectively. The numbering above the alignment is for the sulerythrin sequence. The secondary structures and their designations are shown above sulerythrin and below Rbr; arrows and coils represent the β-strands and α-helices, respectively. S_tokodaii_SulE, sulerythrin (*Sulfolobus tokodaii* ORF st2370); SS02642, *Sulfolobus solfataricus* ORF ss2642; P_furiosus_rbr, *Pyrococcus furiosus* ORF pf1283; PAB0598, *Pyrococcus abyssi* ORF pab598; D_vulgaris_ngr, *Desulfovibrio vulgaris* nigerythrin; D_vulgaris_rbr, *Desulfovibrio vulgaris* rubrerythrin.

Fe and 0.34 mol of Zn per monomer in one preparation, and 1.0 mol of Fe and 0.65 mol of Zn per monomer in another preparation. Here we report the crystal structure of sulerythrin at 1.7 Å resolution.

MATERIALS AND METHODS

The sulerythrin protein was purified from *S. tokodaii* strain 7 cells as described previously (*26*). A preparation of sulerythrin containing 1.0 mol of Fe and 0.65 mol of Zn per monomer was used for this study. The crystals were grown at 25 °C in 1 day by the hanging-drop vapor-diffusion method. A 10 μL drop was made by mixing a reservoir solution and a protein solution (50 mg/mL sulerythrin in 5 mM Tris-HCl, pH 8.0). The drop was equilibrated against a 1 mL reservoir solution comprising 2.0 M ammonium sulfate and 10 mM HEPES−NaOH buffer, pH 7.5. The color of the crystals was brown, and no change of the color was observed after the data collection. Before data collection, the crystals were transferred to a solution containing 20% glycerol in addition to the reservoir solution. The concentration of cryoprotectant was increased by 5% in each step, with equilibration for 3 min between the steps. The data were collected with a CCD camera on the BL6A and BL18B stations of the Photon Factory, High Energy Accelerator Research Organization (KEK), or with a R-axis IV^{++} system on a X-ray generator UltraX18 (Rigaku Corp.). All data were collected at 100 K. Diffraction images were indexed, integrated and scaled using the DPS/MOSFLM program suite (*28*, *29*) or CrystalClear 1.3 (Rigaku Corp.). The crystal belonged to space group $P6_3$ with unit cell dimensions of $a = b = 72.4$ Å and $c = 98.2$ Å. The data collection and processing statistics are given in Table 1. The data collected at the wavelength of 1.000 Å were used for subsequent molecular replacement and crystallographic refinement. Molecular replacement was performed with MOLREP (*30*) in the CCP4 program suite. ARP/wARP (*31*) was used for automatic model building. Model correction in the electron density map was performed with the XtalView program suite (*32*). Refinement was performed with CNS 1.1 (*33*). The refinement statistics are given in Table 2. The final model of the sulerythrin crystal structure contains residues Asp3-Gly143 of chain A, Asp3-Gln139 of chain B, two Fe^{3+} ions, two Zn^{2+} ions, two O_2 molecules, and 351 water molecules. The figures were generated using ESPript (*34*), XFIT in the XtalView program suite, MOLSCRIPT (*35*), Raster3D (*36*), and SPOCK (*37*). The molecular surfaces shown in Figure 5 were calculated using SPOCK.

Table 1: Data and Wavelength Statistics

parameter	data		
wavelength (Å)	1.0000	1.5418	1.7391
facility	PF−BL6A	R-axis	PF−BL18B
exposure time of each frame (s)	20	600	30
no. of frames	90	112	180
unit cell dimensions (Å)			
$a = b$	72.4	72.4	72.4
c	98.2	98.0	97.9
resolution limit (Å)	24.25−1.70	38.58−2.02	33.90−2.75
last shell (Å)	1.79−1.70	2.09−2.02	2.90−2.75
no. of total reflections	171,729	65,643	65,582
no. of unique reflections	32,087	18,957	7,095
R_{merge}[a] (%)	5.4	6.4	3.3
of last shell	34.6	19.5	4.5
$I/\sigma(I)$	10.1	9.3	16.3
of last shell	2.2	3.5	15.1
completeness (%)	99.8	99.2	99.9
of last shell	99.3	100.0	99.5

[a] $R_{merge} = \sum\sum |I_i - \langle I \rangle| / \sum \langle I \rangle$.

Table 2: Refinement Statistics

resolution range (Å)	24.29−1.70
no. of reflections used	32061
R-factor (%)	19.2
R_{free}[a]	22.3
no. of atoms	
protein	2195
solvent sites	351
heteroatoms	8
average B-factor (Å^2)	19.6
Ramachandran plot (%)	
most favored	96.6
allowed	3.4
disallowed	0.0
Rmsd from ideal values	
bond length (Å)	0.005
bond angle (°)	1.1
coordinate error[b] (Å)	0.18

[a] Calculated using a test data set; 5% of total data randomly selected from the observed reflections. [b] Estimated coordinate error from a Luzzati plot.

RESULTS

Crystallography and Overall Structure. The crystal structure of sulerythrin was solved by means of molecular replacement, using the N-terminal four-helix bundle domain (Lys2-Arg140) of 2Fe−Rbr$_{ox}$ (PDB entry 1RYT). The two four-helix bundles in the asymmetric unit were bundled like in the case of the head-to-head dimer of the Rbr (*21*). These subunits were related by a pseudo 2-fold axis of the noncrystallographic symmetry. Automatic chain tracing and building of side chains using the deduced amino acid sequence of ORF st2370 were successfully conducted using the ARP/wARP program. At the automatic chain tracing step, domain swapping of the two chains of the sulerythrin dimer was revealed (Figure 2). Helices αA (Lys8-Glu37) and αB

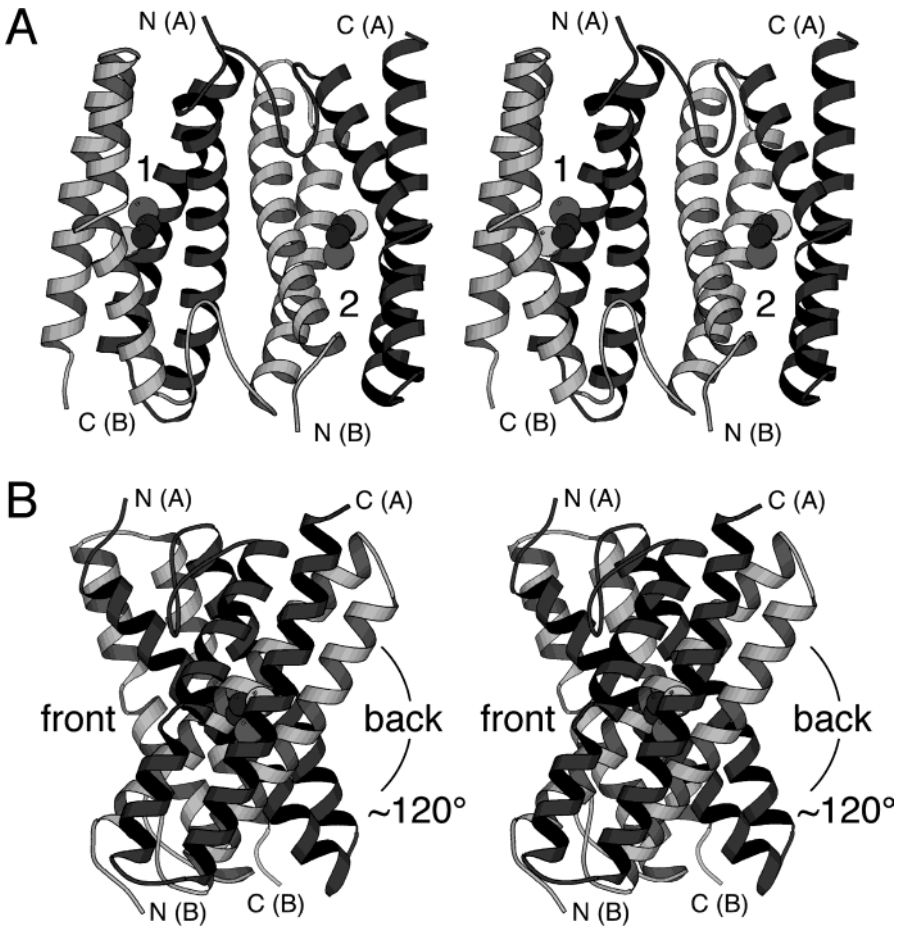

FIGURE 2: Stereographic ribbon diagram of the domain-swapped sulerythrin dimer. Zn, Fe, and oxygen atoms of putative O_2 are denoted by light gray, dark gray, and black spheres, respectively. Chains A and B are shown in dark and light gray. The N- and C-termini of both chains are labeled. (A) Viewed from the "front" side. Binuclear metal center sites 1 and 2 are labeled. (B) The view is rotated 90° around the perpendicular axis from that in panel A. The "front" and "back" sides of the molecules are labeled. The angle between the long axes of the two four-helix bundles is about 120°.

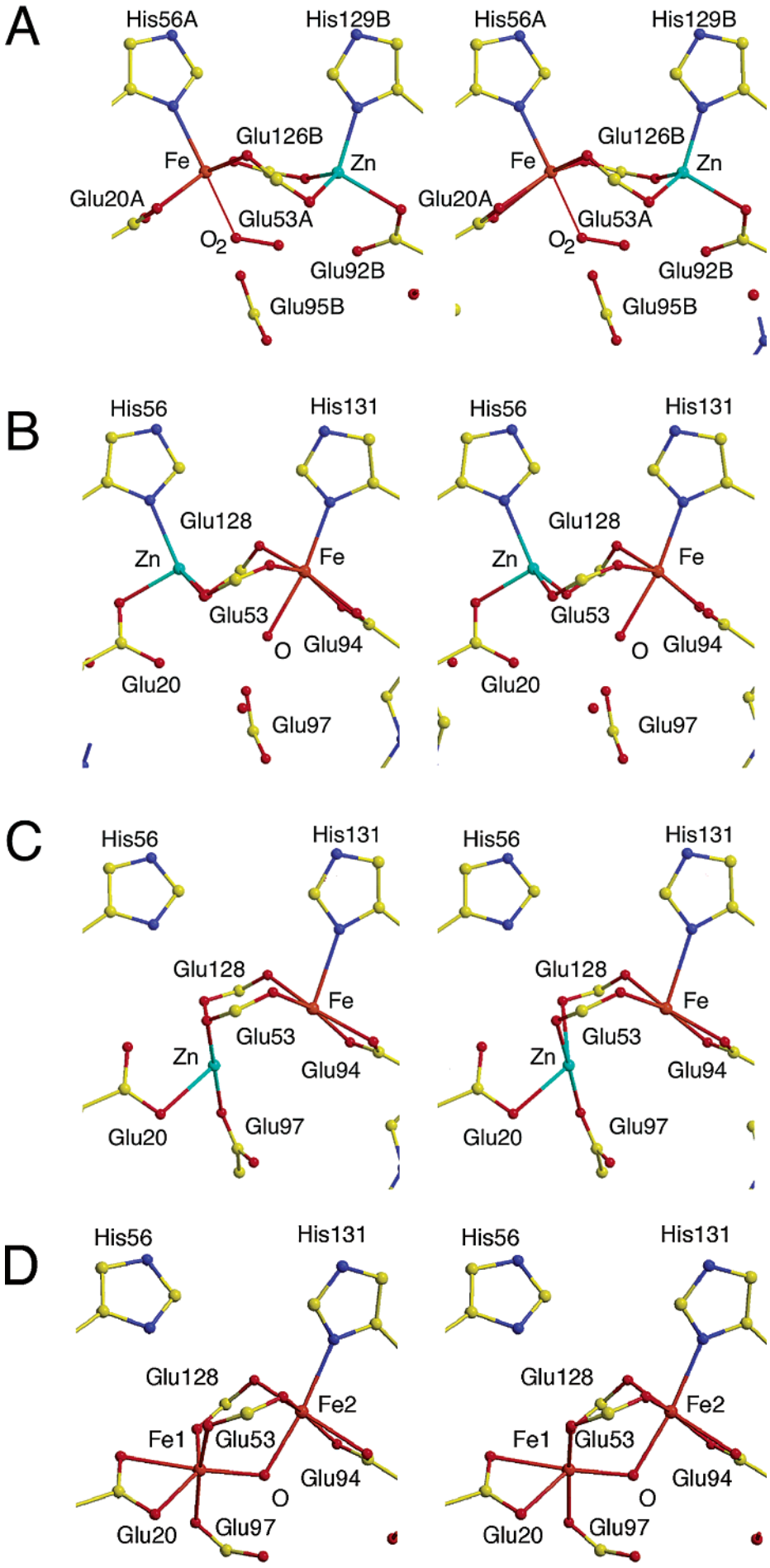
A
His56A
His129B
Glu126B
Fe
Zn
Glu20A
Glu53A
O_2
Glu92B
Glu95B
B
His56
His131
Glu128
Zn
Fe
Glu53
O
Glu94
Glu20
Glu97
C
His56
His131
Glu128
Fe
Glu53
Zn
Glu94
Glu20
Glu97
D
His56
His131
Glu128
Fe2
Fe1
Glu53
Glu94
O
Glu20
Glu97

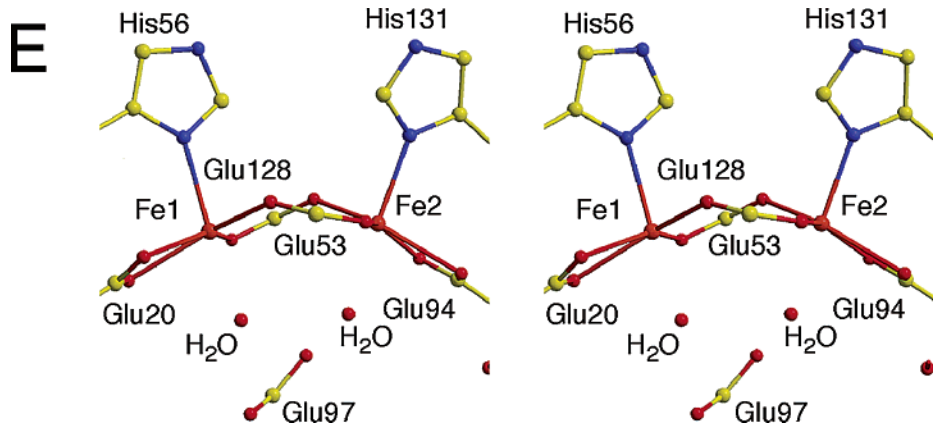

FIGURE 3: Structures of the binuclear metal centers of sulerythrin and Rbr. Stereoviews of the binuclear metal centers in (A) sulerythrin, (B) Fe/Zn−Rbr_{aero} (1DVB), (C) Fe/Zn−Rbr_{anaero} (1JYB), (D) 2Fe−Rbr_{ox} (1LKM), and (E) 2Fe−Rbr_{red} (1LKO). Carbon atoms are yellow, oxygen atoms and waters are red, nitrogen atoms are dark blue, iron atoms are orange, and zinc atoms are light blue.

(Pro40-Glu66) of one chain formed a hybrid four-helix bundle with helices αC (Leu81-Glu109) and αD (Pro113-Gly142) of another chain. The electron density of the loop connecting αB and αC (Gly67-Gly80) was unambiguously continued. The average temperature factors of this region (18.8 and 19.0 Å^2 for chains A and B) were not greatly different from that of the whole polypeptides (17.5 Å^2). In this region, *Sulfolobus* proteins are shorter by 2−3 residues than those from *D. vulgaris* Rbr and nigerythrin, and exhibit no similarity (Figure 1). In some structures of Rbr, the peptide between residues Gly78 and Ile79 in this region is in the *cis* conformation (*22*, *24*). We designate the binuclear metal center, which consists of helices αA/B of chain A and helices αC/D of chain B, as site 1, and the other as site 2 (Figure 2A). The two chains, as well as the two sites, have almost identical structures. As for the region of Leu4-Leu137 of chains A and B, the root-mean-square deviations for Cα atoms and all atoms were 0.19 and 0.85 Å, respectively. Therefore, we mainly describe site 1, unless otherwise noted.

Helix αC was distorted at the position of Gln98 like in the case of Rbr. The four-helix bundle structure of sulerythrin was a hybrid of two chains, but was very similar to that of Rbr, which consists of a single chain. The root-mean-square deviations of Cα atoms in the four-helix bundle domain between sulerythrin (2−64 and 81−141 of different chains) and all Rbr structures (2−64 and 79−139) were all within the range of 0.68−0.78 Å. The angles between the long axes of the two four-helix bundles of the sulerythrin dimer and the head-to head dimer of Rbr were also similar, being about 120° (Figure 2B). The dimer interface mainly consists of two parts; a strong interface in the hybrid four-helix bundle between αA/B and αC/D, and a weak interface between the two bundles. The latter mainly involves hydrophilic interactions between the C-terminal half of αA and the loop connecting αB and αC. Five hydrogen bonds, Arg25A-Thr54B, Tyr29A-Arg62B, Arg26A-Arg71B, and Arg33A-Gly79B, are formed in this region.

Metal Binding Site. From the first stage of the crystallographic refinement, two large peaks were observed at the positions corresponding to the Fe and Zn sites of Fe/Zn−Rbr_{aero}, and also to the two Fe sites of 2Fe−Rbr_{red}. In the Fe/Zn−Rbr_{aero} structure, the Fe site (designated as site A) is formed by Glu94 and His131, and the Zn site (site B) by Glu20 and His56 (*24*) (Figure 3B). To identify the metals in the crystal structure of sulerythrin by means of anomalous scattering analysis, we collected data at three different wavelengths (Table 1). A Bijvoet difference density map of the data collected at the wavelength of 1.0000 Å showed strong peaks for both sites (Figure 4A, 40σ and 26σ high). On the other hand, difference density maps of the data collected at wavelengths above the absorption edge of Zn showed a strong peak only for site B (12σ at $\lambda = 1.5418$ Å and 30σ at $\lambda = 1.7400$ Å), but site A showing greatly reduced anomalous scattering ability (Figure 4B,C). This indicates that the metal sites of sulerythrin were inverted compared to those of Fe/Zn−Rbr_{aero}, as to the positions of Fe and Zn. Although the oxidation state of Fe atom is not definitive yet, we tentatively treated the atom as ferric ions (Fe^{3+}) during crystallographic refinement, according to the brownish color of the crystals. Crystallographic refinement of ferric ions (Fe^{3+}) and zinc ions (Zn^{2+}) revealed no unusual behavior of the temperature factors for these atom assignments (Table 3A). The occupancies of the ferric ions were fixed at 1.0, because the values did not change on the refinement. On the other hand, the occupancies of the zinc ions were refined to be 0.87 and 0.80 for sites 1 and 2, respectively. The Oϵ1 atom of Glu92 is not liganded to the Zn atom, and the electron density maps for the atoms in both chains were ambiguous (Figure 4E). The temperature factors of the Glu 92 Oϵ1 atoms in chains A and B were significantly higher than those of Oϵ2 atoms of the same residues (Table 3A), being 38.4 and 32.2 Å^2, respectively. The temperature factors of the carboxylate atoms coordinating the Zn atoms were slightly higher than those coordinating the Fe atoms (Table 3A), probably because about 20% of the molecules in the crystal do not coordinate the Zn^{2+} ion.

At the positions corresponding to sites C and D of Rbr, electron density corresponding to two connected light atoms (such as carbon, nitrogen, and oxygen) was observed (Figure 4D−F). We tentatively included an O_2 molecule at the site for the crystallographic refinement, because the sulerythrin crystal was prepared aerobically throughout the purification and crystallization steps. The temperature factors and occupancies of these putative O_2 atoms were individually refined, but converged within ranges of 20−23 Å^2, and 0.73−0.88, respectively (Table 3A). The refined occupancies of putative O_2 atoms were not greatly different from those of Zn atoms. This suggests that only the Zn^{2+}-containing

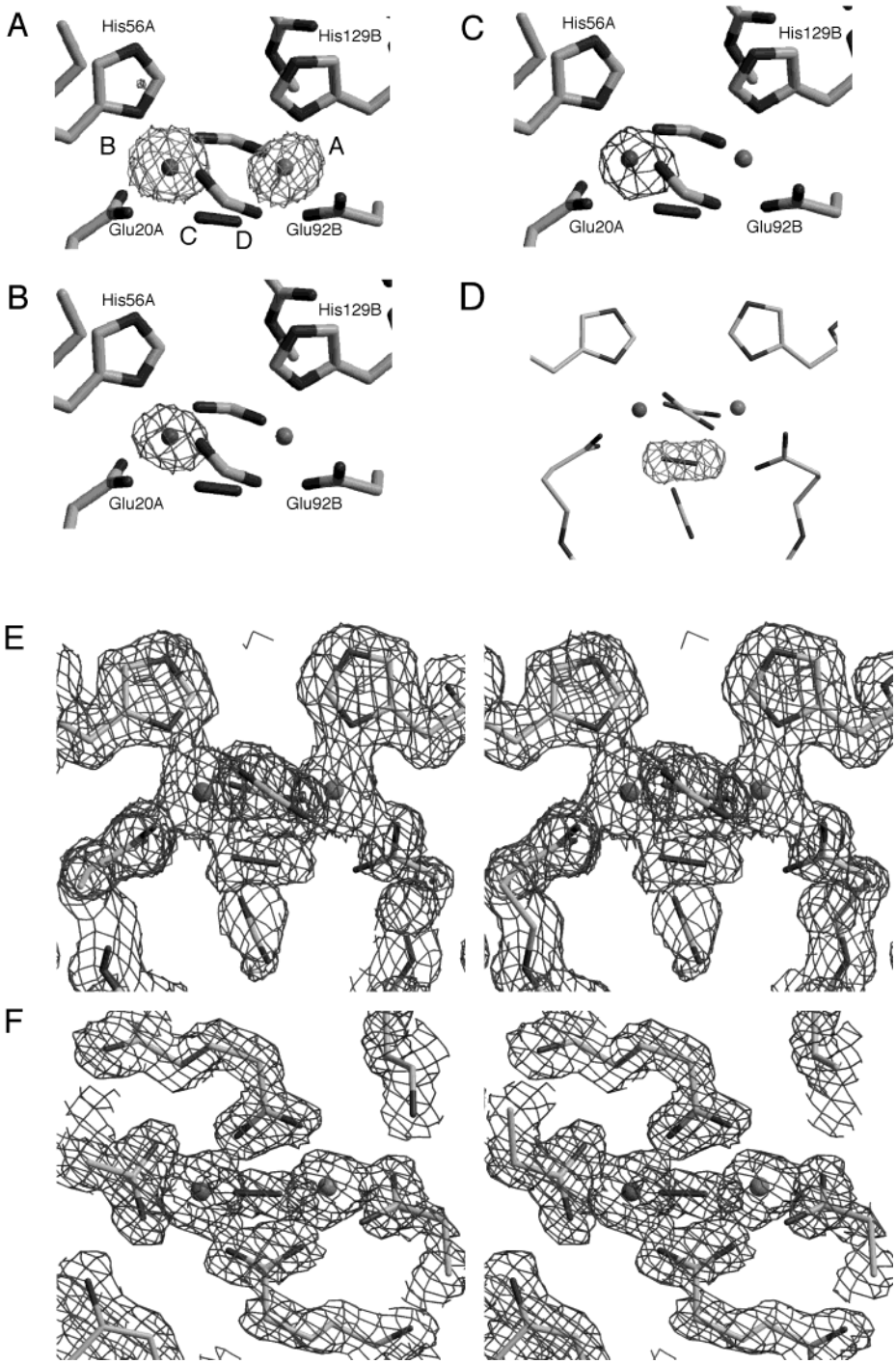

FIGURE 4: Electron density maps of sulerythrin at the binuclear metal center. Site 1 is shown. (A−C) Difference electron densities ($|F_o| - |F_c|$). The final model, and labels for Glu20A, His56A, Glu92B, and His129B are shown. (A) Data collected at the wavelength of 1.0000 Å contoured at 6σ. Labels A to D indicate the approximate positions of the sites defined in ref *24*. (B) Data collected at the wavelength of 1.5418 Å contoured at 6σ. (C) Data collected at the wavelength of 1.7400 Å contoured at 16σ. (D) $|F_o| - |F_c|$ omit map for the putative O_2 molecule of the final model contoured at 6σ. (E, F) Stereoviews of the final model and $2|F_o| - |F_c|$ maps contoured at 2σ. The view in panel F is rotated 90° around the horizontal axis from that in panel E.

molecules in the crystal can bind the ligand, if they are composed of oxygen atoms or atoms with similar scattering capabilities.

However, there is another possibility that two water molecules or ions with partial occupancies are bound. The O−O distance of putative O_2 molecules at sites 1 and 2 were refined to be 1.25 and 1.26 Å, respectively, under the restraint of 1.248 Å. In the absence of restraint, the distances were converged within a range of 1.1−1.6 Å. The distance between Fe and O1 atom of the putative O_2 molecule was 2.2 Å in average (Table 3B). Perhaps an $Fe^{2+}-O_2$ adduct formed in the crystal during the data collection, resulting from reduction of iron in the synchrotron beam. However, the color of the crystal did not appear to change before and after the data collection. There is one more alternative possibility, namely, that partial reduction in the X-ray beam formed a mixture of Fe^{2+} and Fe^{3+}, resulting in two different Fe−O distances of bound water molecules. The distances between Fe and farther O atom (O2) of the putative O_2 molecule were 3.0 and 3.2 Å in sites 1 and 2, respectively.

Table 3: Metal Binding Sites of Sulerythrin

(A) Occupancies and Temperature Factors of the Metal and Ligand Atoms

site 1	occupancy	B-factor (Å^2)	site 2	occupancy	B-factor (Å^2)
Fe401	1.00[a]	16.3	Fe404	1.00[a]	15.7
Zn402	0.87	26.3	Zn405	0.80	22.2
$O_2$403 O1	0.83	20.7	$O_2$406 O1	0.73	22.5
$O_2$403 O2	0.85	23.2	$O_2$406 O2	0.88	21.3
Glu53A Oϵ1	1.00[a]	18.8	Glu53B Oϵ2	1.00[a]	19.0
Glu20A Oϵ1	1.00[a]	15.8	Glu20B Oϵ1	1.00[a]	17.8
Glu20A Oϵ2	1.00[a]	23.2	Glu20B Oϵ2	1.00[a]	12.5
Glu126B Oϵ2	1.00[a]	23.5	Glu126A Oϵ2	1.00[a]	24.4
His56A Nδ1	1.00[a]	17.8	His56B Nδ1	1.00[a]	14.4
Glu92B Oϵ2	1.00[a]	24.8	Glu92A Oϵ2	1.00[a]	23.3
Glu53A Oϵ2	1.00[a]	26.8	Glu53B Oϵ2	1.00[a]	21.9
Glu126B Oϵ1	1.00[a]	25.0	Glu126A Oϵ1	1.00[a]	21.3
His129B Nδ1	1.00[a]	16.4	His129A Nδ1	1.00[a]	12.4

(B) Distances (Å) and Angles (°) of the Metal Binding Sites in Suleythrin and Aerobically Prepated *D. vulgaris* Rubrerythrin Containing Fe/Zn (FeZn-Rbr_{aero})

metal−ligand distances (Å)			metal−ligand distances (Å)	
sulerythrin	site 1	site 2	rubrerythrin[b]	
Fe−O1 (O_2)	2.12	2.35	Fe−O (water 196)	2.20
Fe−Oϵ1 Glu53	2.11	2.06	Fe−Oϵ2 Glu53	2.04
Fe−Oϵ1 Glu20	2.38	2.36	Fe−Oϵ1 Glu94	2.06
Fe−Oϵ2 Glu20	2.15	2.07	Fe−Oϵ2 Glu94	2.03
Fe−Oϵ2 Glu126	1.98	1.95	Fe−Oϵ1 Glu128	2.02
Fe−Nδ1 His56	2.14	2.07	Fe−Nδ1 His131	2.18
Zn−Oϵ2 Glu92	2.12	2.06	Zn−Oϵ2 Glu20	2.10
Zn−Oϵ2 Glu53	2.16	1.96	Zn−Oϵ1 Glu53	2.10
Zn−Oϵ1 Glu126	2.01	2.05	Zn−Oϵ2 Glu128	2.09
Zn−Nδ1 His129	1.96	1.98	Zn−Nδ1 His56	2.20
ligand−metal-ligand angles (°)			ligand−metal-ligand angles (°)	
O1 (O_2)−Fe193−Oϵ1 Glu53	91.7	86.3	O(water 196)−Fe193−Oϵ2 Glu53	75.5
O1 (O_2)−Fe193−Oϵ1 Glu20	82.9	84.0	O(water 196)−Fe193−Oϵ1 Glu94	83.6
O1 (O_2)−Fe193−Oϵ2 Glu20	76.6	80.0	O(water 196)−Fe193−Oϵ2 Glu94	79.6
O1 (O_2)−Fe193−Oϵ2 Glu126	84.1	78.8	O(water 196)−Fe193−Oϵ1 Glu128	93.4
O1 (O_2)−Fe193−Nδ1 His56	170.3	170.6	O(water 196)−Fe193−Nδ1 His131	166.5
Oϵ1 Glu53−Fe−Oϵ2 Glu20	145.0	141.8	Oϵ2 Glu53−Fe−Oϵ1 Glu94	151.8
Oϵ1 Glu53−Fe−Oϵ2 Glu20	88.5	84.5	Oϵ2 Glu53−Fe−Oϵ2 Glu94	97.9
Oϵ1 Glu53−Fe−Oϵ2 Glu126	116.3	123.6	Oϵ2 Glu53−Fe−Oϵ1 Glu128	102.0
Oϵ1 Glu53−Fe−Nδ1 His56	96.9	99.4	Oϵ2 Glu53−Fe−Nδ1 His131	91.7
Oϵ1 Glu20−Fe−Oϵ2 Glu20	57.6	58.8	Oϵ1 Glu94−Fe−Oϵ2 Glu94	59.4
Oϵ1 Glu20−Fe−Oϵ1 Glu126	95.6	88.5	Oϵ1 Glu94−Fe−Oϵ1 Glu128	97.8
Oϵ1 Glu20−Fe−Nδ1 His56	98.6	99.5	Oϵ1 Glu94−Fe−Nδ1 His131	109.9
Oϵ2 Glu20−Fe−Oϵ1 Glu126	152.3	145.3	Oϵ2 Glu94−Fe−Oϵ1 Glu128	156.5
Oϵ2 Glu20−Fe−Nδ1 His56	101.7	103.9	Oϵ2 Glu94−Fe−Nδ1 His131	106.8
Oϵ2 Glu126−Fe−Nδ1 His56	88.1	91.9	Oϵ1 Glu128−Fe−Nδ1 His131	85.1
Oϵ2 Glu92−Zn−Oϵ2-Glu53	95.4	92.9	Oϵ2 Glu20−Zn−Oϵ1 Glu53	107.3
Oϵ2 Glu92−Zn−Nδ1 His129	103.6	112.9	Oϵ2 Glu20−Zn−Nδ1 His56	97.8
Oϵ2 Glu92−Zn−Oϵ1 Glu126	113.8	119.0	Oϵ2 Glu20−Zn−Oϵ2 Glu128	97.4
Oϵ2 Glu53−Zn−Nδ1 His129	116.6	107.2	Oϵ1 Glu53−Zn−Nδ1 His56	118.8
Oϵ2 Glu53−Zn−Oϵ2 Glu126	121.9	130.3	Oϵ1 Glu53−Zn−Oϵ2 Glu128	115.8
Nδ1 His129−Zn−Oϵ2 Glu126	104.4	94.7	Nδ1 His56−Zn−Oϵ2 Glu128	120.4

[a] Not refined. [b] Values taken from ref *24*.

However, current crystallographic resolution is not high enough to confirm these possibilities. The distances between Zn and O2 atom of the putative O_2 molecule were 2.7 and 2.5 Å in sites 1 and 2, respectively. Oϵ1 of Glu 95 was very close to both O1 and O2 atoms of the putative O_2 molecule (2.6 Å to both O1 and O2 in both sites 1 and 2). Oϵ1 of Glu92 was also close to O2 atom of the putative O_2 molecule (2.5 and 2.9 Å in sites 1 and 2, respectively). These hydrogen-bonding distances indicate that either the Glu residue or the ligand atom is protonated. Because Glu residues are unlikely protonated at pH 7.5, it is again suggested that a disordered water is present. There was no interaction with the putative O_2 molecule other than those of the metal ions, metal-coordinating residues, and Glu95.

Glu 53 and Glu126 formed bridges between Fe and Zn atoms by coordinating them, but angles of the carboxyl planes of these residues were different from those in all Rbr structures (Figure 3). As a result, the Fe^{3+} ion was octahedrally hexacoordinated in a slightly distorted manner, by Oϵ1 and Oϵ2 of Glu20A, Oϵ1 of Glu53A, Oϵ2 of Glu 126, Nδ1 of His56A, and the O1 atom of the O_2 molecule. The Zn^{2+} ion was tetrahedrally coordinated by Oϵ2 of Glu53, Oϵ2 of Glu92, Oϵ1 of Glu126, and Nδ1 of His129. Thus, the binuclear metal center of sulerythrin was asymmetric, unlike that of 2Fe−Rbr_{red} (Figure 3E) (*22*). The distances and angles formed by the metal and ligand atoms are shown

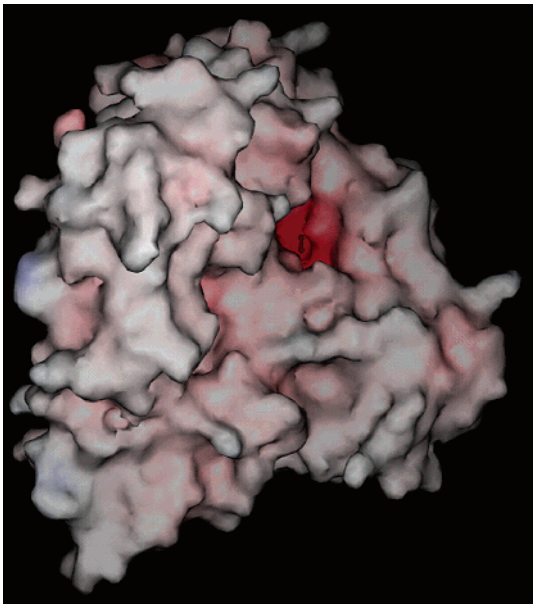

FIGURE 5: Molecular surface of sulerythrin, calculated using the SPOCK program with a probe radius of 1.4 Å. According to the electrostatic potential, the surface is colored blue for positive and red for negative charges. The putative O_2 molecule is shown as a ball-and-stick model in dark red.

in Table 3B. The metal binding site of sulerythrin was similar to that of Fe/Zn−Rbr, except for the exchange of the Fe and Zn sites. Hydrogen bonds were formed between Glu20 and Tyr100 (2.6 Å in both sites), and between Glu94 and Tyr27 (2.9 and 2.7 Å in sites 1 and 2). These hydrogen bonds with tyrosine residues are strictly conserved in all rubrerythrin-like proteins. His56 and His 129 of sulerythrin did not form a hydrogen bond at Nϵ2 atoms, unlike in the case of Rbr. In the Rbr structure, His56Nϵ2 is hydrogen-bonded with the main-chain carbonyl of Cys161 near the rubredoxin-like FeS_4 center of the next subunit across the "head-to-tail" dimer interface, but this intersubunit interaction is absent in sulerythrin. The His131 residue of Rbr forms a hydrogen bond with the side-chain carbonyl of Gln52, but the residue is replaced by glycine in sulerythrin (Figure 1).

Because of the distortion of helix αC at Glu98, the two metal binding sites of the sulerythrin molecule are solvent-accessible through a crevice formed between helices αA and αC, facing the same front side (Figure 2). Figure 5 shows the molecular surface and the electrostatic potential of the front side. An O_2 molecule can be seen deep inside the pocket-like cavity. This crevice is lined by mainly hydrophobic residues; Gly16, Gly19, and Ala23 in αA, Ala73 and Thr74 in the loop connecting αB and αC, and Gly91, Tyr94, Glu95, Met99, and Phe103 in αC. The loop connecting αB and αC partly covers the crevice, forming the upper lid of the crevice that can be seen in Figure 5. These residues in αA and αC are relatively conserved among rubrerythrin-like proteins. Although the crevice is hydrophobic, some water molecules existed in the cavity under the loop connecting αB and αC.

DISCUSSION

The domain-swapped dimer structure of sulerythrin should reflect the structure in vivo, because the sample is "as isolated" from *S. tokodaii* strain 7. Several examples of artificially obtained domain-swapped oligomers, such as at a nonphysiologically low pH, are reported (*38*). However, the domain-swapped dimer of sulerythrin does not easily dissociate, because strong interchain interactions are formed in the hybrid four-helix bundles. Even with the high ammonium sulfate concentration of the crystallization conditions, the tightly bundled helices, αA/B and αC/D, does not seem to dissociate. Another four-helix bundled proteins, ferritins show plasticity of the ferroxidase di-iron active sites in the same protein family, but not by domain swapping (*39*). In classical ferritins, the di-iron center is located in a four-helix bundle core. In *Listeria innocua* ferritin, the di-iron center is located at the interface between two subunits related by 2-fold symmetry. The di-iron center is composed of only two N-terminal helices (αA and αB), i.e., two C-terminal helices (αC and αD) are not involved. Despite the differences in location, the di-iron centers of classical and *L. innocua* ferritins are chemically and structurally similar. The domain swapping found in the sulerythrin structure may also be one of the possible mechanisms for generating plasticity of protein active sites (*40*). Four-helix bundled diiron proteins can be designed with units of two helices. De novo design of a hybrid protein consisting of two discreet monomers has been reported (*41*).

Interestingly, the binuclear metal center of sulerythrin in this study was not similar to any known states of the site in Rbr, but the metal sites were switched compared to those of Fe/Zn−Rbr_{aero}. It has been suggested that the binuclear metal binding site of Rbr is capable of binding di-iron or Fe/Zn without undergoing large structural changes, with two states for each metal composition (*22*, *25*). Here we can suggest that the site is more flexible, the positions of Fe and Zn being switched through the rotation of bridging Glu53 and Glu126 residues. The unusually high flexibility of the site explains the many different activities ascribed to Rbr.

The characteristics of sulerythrin are comparable with to those of Fe/Zn−Rbr_{aero}. The occupancies of the Zn atoms in the crystal structure of sulerythrin were considerably lower than those of the Fe atoms. In our previous study, the content of Zn was shown vary in individual preparations, down to 0.34 mol per monomer (*26*), indicating that the Zn site is labile. These results coincide with the report showing the movement of the Zn site of Fe/Zn−Rbr under aerobic conditions (*25*). However, sulerythrin binds an undefined ligand, and does not show inorganic pyrophosphatase activity, unlike Fe/Zn−Rbr_{aero} (*26*). Although we observed Fe/Zn binuclear metal binding site of sulerythrin crystals in this study, the protein solution shows similar UV absorption spectrum to "chopped" rubrerythrin (*26*), which has diferric-oxo bridged site. It is possible that there exist other soluble species than the present crystal structure. Difference of net charge at the binuclear metal binding center could influence on crystal formation, although the site is not directly involved in the crystal packing. In this study, an O_2 molecule was tentatively assigned to the electron density observed at the binuclear metal center, but identity of the molecule (or atoms) is not confirmed yet. It was suggested that sulerythrin binds azide, on the basis of absorption spectra (*26*). Further investigation on the characteristics of the binuclear metal binding site of sulerythrin is needed.

The domain swapping of sulerythrin may be the cause of the different properties of its binuclear metal center from

those of Rbr. These properties may be caused also by the absence of a hydrogen bond at the Nϵ2 atoms of the two histidine ligands (His56 and His129). The Gln52 residue of Rbr is not conserved in rubrerythrin-like proteins of *Sulfolobus* and *Pyrococcus* species, or nigerythrin (Figure 1). Therefore, the binuclear metal centers of these proteins may also have different properties from those of Rbr. Although the crystal structures of rubredoxin-like proteins from *Pyrococcus* species are not available, these proteins, whose loops connecting αB and αC are very short, are expected not to be domain-swapped. As to 2Fe−Rbr_{red}, intersubunit electron transfer from the rubredoxin-like FeS_4 center to the binuclear metal center across the "head-to-tail" dimer interface is suggested to be important for its hydrogen peroxidase activity (*22*). On the other hand, sulerythrin only forms a "head-to-head" dimer and lacks the rubredoxin-like FeS_4 domain.

ACKNOWLEDGMENT

We wish to thank the staff of the Photon Factory for their assistance with the data collection.

REFERENCES

1. LeGall, J., Prickril, B. C., Moura, I., Xavier, A. V., Moura, J. J., and Huynh, B. H. (1988) *Biochemistry 27*, 1636−42.
2. Prickril, B. C., Kurtz, D. M., Jr., LeGall, J., and Voordouw, G. (1991) *Biochemistry 30*, 11118−23.
3. Lehmann, Y., Meile, L., and Teuber, M. (1996) *J. Bacteriol. 178*, 7152−8.
4. Das, A., Coulter, E. D., Kurtz, D. M., Jr., and Ljungdahl, L. G. (2001) *J. Bacteriol. 183*, 1560−7.
5. Sztukowska, M., Bugno, M., Potempa, J., Travis, J., and Kurtz, D. M., Jr. (2002) *Mol. Microbiol. 44*, 479−88.
6. Lumppio, H. L., Shenvi, N. V., Garg, R. P., Summers, A. O., and Kurtz, D. M., Jr. (1997) *J. Bacteriol. 179*, 4607−15.
7. Pierik, A. J., Wolbert, R. B., Portier, G. L., Verhagen, M. F., and Hagen, W. R. (1993) *Eur. J. Biochem. 212*, 237−45.
8. Le Gall, J., Payne, W. J., Chen, L., Liu, M. Y., and Xavier, A. V. (1994) *Biochimie 76*, 655−65.
9. Liu, M. Y., and LeGall, J. (1990) *Biochem. Biophys. Res. Commun. 171*, 313−8.
10. Bonomi, F., Kurtz, D. M., Jr., and Cui, X. Y. (1996) *J. Biol. Inorg. Chem. 1*, 67−72.
11. Gomes, C. M., LeGall, J., Xavier, A. V., and Teixeira, M. (2001) *Chembiochem. 2*, 583−7.
12. Coulter, E. D., Shenvi, N. V., and Kurtz, D. M., Jr. (1999) *Biochem. Biophys. Res. Commun. 255*, 317−23.
13. Lumppio, H. L., Shenvi, N. V., Summers, A. O., Voordouw, G., and Kurtz, D. M., Jr. (2001) *J. Bacteriol. 183*, 101−8.
14. Coulter, E. D., and Kurtz, D. M., Jr. (2001) *Arch. Biochem. Biophys. 394*, 76−86.
15. Kurtz, D. M., Jr., and Prickril, B. C. (1991) *Biochem. Biophys. Res. Commun. 181*, 337−41.
16. Geissmann, T. A., Teuber, M., and Meile, L. (1999) *J. Bacteriol. 181*, 7136−9.
17. Adams, M. W., Jenney, F. E., Jr., Clay, M. D., and Johnson, M. K. (2002) *J. Biol. Inorg. Chem. 7*, 647−52.
18. Dave, B. C., Czernuszewicz, R. S., Prickril, B. C., and Kurtz, D. M., Jr. (1994) *Biochemistry 33*, 3572−6.
19. Gupta, N., Bonomi, F., Kurtz, D. M., Jr., Ravi, N., Wang, D. L., and Huynh, B. H. (1995) *Biochemistry 34*, 3310−8.
20. Coulter, E. D., Shenvi, N. V., Beharry, Z. M., Smith, J. J., Prickril, B. C., and Kurtz, D. M., Jr. (2000) *Inorg. Chim. Acta 297*, 231−241.
21. deMare, F., Kurtz, D. M., Jr., and Nordlund, P. (1996) *Nat. Struct. Biol. 3*, 539−46.
22. Jin, S., Kurtz, D. M., Jr., Liu, Z. J., Rose, J., and Wang, B. C. (2002) *J. Am. Chem. Soc. 124*, 9845−55.
23. Sieker, L. C., Holmes, M., Le Trong, I., Turley, S., Santarsiero, B. D., Liu, M. Y., LeGall, J., and Stenkamp, R. E. (1999) *Nat. Struct. Biol. 6*, 308−9.
24. Sieker, L. C., Holmes, M., Le Trong, I., Turley, S., Liu, M. Y., LeGall, J., and Stenkamp, R. E. (2000) *J. Biol. Inorg. Chem. 5*, 505−13.
25. Li, M., Liu, M. Y., LeGall, J., Gui, L. L., Liao, J., Jiang, T., Zhang, J. P., Liang, D. C., and Chang, W. R. (2003) *J. Biol. Inorg. Chem. 8*, 149−55.
26. Wakagi, T. (2003) *FEMS Microbiol. Lett. 222*, 33−37.
27. Kawarabayasi, Y., Hino, Y., Horikawa, H., Jin-no, K., Takahashi, M., Sekine, M., Baba, S., Ankai, A., Kosugi, H., Hosoyama, A., Fukui, S., Nagai, Y., Nishijima, K., Otsuka, R., Nakazawa, H., Takamiya, M., Kato, Y., Yoshizawa, T., Tanaka, T., Kudoh, Y., Yamazaki, J., Kushida, N., Oguchi, A., Aoki, K., Masuda, S., Yanagii, M., Nishimura, M., Yamagishi, A., Oshima, T., and Kikuchi, H. (2001) *DNA Res. 8*, 123−140.
28. Steller, I., Bolotovsky, R., and Rossmann, M. G. (1997) *J. Appl. Crystallogr. 30*, 1036−1040.
29. Powell, H. R. (1999) *Acta Crystallogr. D55*, 1690−1695.
30. Vagin, A., and Teplyakov, A. (1997) *J. Appl. Crystallogr. 30*, 1022−1025.
31. Morris, R. J., Perrakis, A., and Lamzin, V. S. (2002) *Acta Crystallogr. D58*, 968−75.
32. McRee, D. E. (1999) *J. Struct. Biol. 125*, 156−65.
33. Brunger, A. T., Adams, P. D., Clore, G. M., DeLano, W. L., Gros, P., Grosse-Kunstleve, R. W., Jiang, J.-S., Kuszewski, J., Nilges, M., Pannu, N. S., Read, R. J., Rice, L. M., Simonson, T., and Warren, G. L. (1998) *Acta Crystallogr. D54*, 905−21.
34. Gouet, P., Courcelle, E., Stuart, D. I., and Metoz, F. (1999) *Bioinformatics 15*, 305−8.
35. Kraulis, P. J. (1991) *J. Appl. Crystallogr. 24*, 946−50.
36. Merritt, E. A., and Bacon, D. J. (1997) *Methods Enzymol. 277*, 505−24.
37. Christopher, J. A., and Baldwin, T. O. (1998) *J. Mol. Graphics Model. 16*, 285.
38. Liu, Y., and Eisenberg, D. (2002) *Protein Sci. 11*, 1285−99.
39. Ilari, A., Stefanini, S., Chiancone, E., and Tsernoglou, D. (2000) *Nat. Struct. Biol. 7*, 38−43.
40. Todd, A. E., Orengo, C. A., and Thornton, J. M. (2002) *Trends Biochem. Sci. 27*, 419−26.
41. Costanzo, L. D., Wade, H., Geremia, S., Randaccio, L., Pavone, V., Degrado, W. F., and Lombardi, A. (2001) *J. Am. Chem. Soc. 123*, 12749−57.

BI034220B